

RSC Advances



This is an *Accepted Manuscript*, which has been through the Royal Society of Chemistry peer review process and has been accepted for publication.

Accepted Manuscripts are published online shortly after acceptance, before technical editing, formatting and proof reading. Using this free service, authors can make their results available to the community, in citable form, before we publish the edited article. This *Accepted Manuscript* will be replaced by the edited, formatted and paginated article as soon as this is available.

You can find more information about *Accepted Manuscripts* in the [Information for Authors](#).

Please note that technical editing may introduce minor changes to the text and/or graphics, which may alter content. The journal's standard [Terms & Conditions](#) and the [Ethical guidelines](#) still apply. In no event shall the Royal Society of Chemistry be held responsible for any errors or omissions in this *Accepted Manuscript* or any consequences arising from the use of any information it contains.

ARTICLE

Growth kinetics of gold nanoparticles on silica/graphene surfaces for multiplex biological immunoassays

Cite this: DOI: 10.1039/x0xx00000x

Received 00th March 2014,
Accepted 00th March 2014

DOI: 10.1039/x0xx00000x

www.rsc.org/

Rouslan V. Olkhov^a and Andrew M. Shaw^{a*}

Kinetics of seed-mediated chemical growth of gold nanoparticles on silica substrates coated with a thin layer of graphene-derivative materials were studied with ultimate goal of employing the developed graphene-nanoparticle composites in light-scattering imaging biosensor applications. The type of the surface coating and chemical conditions influence the surface number density and size of the grown nanoparticles. Importantly, when used as biosensor bases, the substrates coated with protein reduced graphene oxide have shown beneficial biological compatibility towards immobilized antibodies resulting in about 20-fold improvement in antigen capture by the antibodies tethered to the sensor surface in immunoassay performed on the multiplex photonic biosensor platform.

Introduction

Microarray based high-throughput analytical techniques are inevitable in the fields of genomics, proteomics and glycomics. Evolving personalized medicine diagnostics also relies on rapid proteomic profiling by microarray format biosensors¹. Point-of-care devices required for personalized diagnostics are expected to develop through miniaturization and multiplexing. Although mass spectrometry methods remain ultimate in data quality, the associated cost and clinical sample separation challenges limit its widespread adoption as a diagnostic technique. Quantitative microarray based analytical tools can complement and supplement the mass spectrometry^{2, 3}. Biosensor platforms that use the optical properties of nanoparticles as the detection event have recently attracted increasing attention in these fields⁴.

The optical properties of nanoparticles associated with graphene surfaces are altered and nanoparticle/graphene composite materials have been explored by some for biosensor applications⁵⁻⁸. The sensor performance enhancements are attributed not only to unique physical properties of graphene (fast electron transfer and large surface area) as a substrate/support for nanoparticles, but synergistic effects are also observed⁹⁻¹². Although the progress in nanoparticle/graphene composite manufacturing is evident¹³⁻¹⁸, the subject is still largely restricted to qualitative studies and underdeveloped: each particular application must be optimized in terms of nanoparticle-graphene assembly structure as well as

microscopic properties of the nanoparticles, their material composition, shape and size^{13, 19, 20}.

There are two extremes in the approach of nanoparticle/graphene composite synthesis: create the composite by deposition of separately synthesised nanoparticles onto graphene material; or direct, spontaneous formation of the nanoparticles by reduction of gold ions in the presence of the graphene material. The former offers better control over the particle formation process but involves more synthetic steps, including particle-graphene tethering, while the latter has synthetic challenges to control the shape and size distributions of the resulting nanoparticles^{13, 21}. A combination of these two methods is a seed-mediated growth of small nanoparticles associated with the graphene surface, which improves control over the particle formation process. The majority of studies on nanoparticle/graphene composites adopt the former separate synthesis approach^{14, 22-24}, with only a few studies exploring *in situ* growth observations at the solid-liquid interface²⁵.

The seeded growth process also offers an interesting option for the sensor manufacture: the control over the spatial distribution of the nanoparticles on the sensor surface, essential to the manufacture of biosensors in a microarray format. In this paper, we present the results of a kinetic study of the seed-mediated growth of gold nanoparticles on several graphene material coated silica substrates. The resulting composite materials are tested in label-free protein immunoassay arrays.

Materials and Methods

Chemicals and Materials

Auric chloride (Tetrachloro auric(III) acid, $\text{HAuCl}_4 \cdot 3\text{H}_2\text{O}$, 99.9%), silver nitrate (AgNO_3 , 99%), cetyltrimethylammonium bromide (CTAB, 95%), sodium citrate ($\text{C}_6\text{H}_5\text{Na}_3\text{O}_7 \cdot 2\text{H}_2\text{O}$, 99.9%), bovine serum albumin (BSA, 98%), fibrinogen (FG, protein content 60%), methyl blue dye (MB) were obtained from Sigma-Aldrich; sodium borohydride (NaBH_4 , 98%) was from Lancaster; (L+) ascorbic acid ($\text{C}_6\text{H}_8\text{O}_6$, 99%) was from Acros; dithiobis-succinimidyl propionate (DTSP, 97%) was from Fluka. Glass slides coated with aminoalkylsilane, (Silane-Prep Slides) were from Sigma-Aldrich. Human transferrin, TRA (4 mg/mL) was obtained from Invitrogen; goat polyclonal antibody to CRP, aCRP (10 mg/mL IgG fraction), were from Abcam; sheep polyclonal antibodies to TRA, aTRA (34.3mg/mL, IgG fraction), were supplied by AbD Serotec. Graphene oxide (GO) was supplied by Sigma-Aldrich. The protein and antibody solutions were prepared and used in standard phosphate buffered saline, PBS, containing 0.005 wt% Tween 20 surfactant, supplied by Sigma-Aldrich. Throughout the experiments 18 M Ω cm de-ionized water was used as solvent when required, and 100 mM phosphoric acid solution was used as regeneration buffer.

Substrate Preparation

Three reduced graphene oxide (rGO) samples were prepared by reducing GO using BSA and FG proteins according to procedure described by Liu et al.²⁶, and using MB as suggested by Cai et al.²⁷, synthesis details are provided in supplemental materials. All three prepared rGO samples and the original GO were purified of the residual water-soluble chemicals by repeated centrifugation cycles, discarding the supernatant and re-suspending the sample in pure water. The changes associated with reduction of GO are clearly visible as sample colour change: the original brown-yellow GO turns into black BSA/FG-rGO or blue-black MB-rGO suspension. The samples were stable as water suspensions for several weeks after preparation. Both protein reduced graphene oxide coated substrates showed very similar behaviour in the subsequent experiments and only the BSA-rGO data and analysis are presented.

The aminated silane glass slides (ASG) were immersion-coated with GO, BSA-rGO, FG-rGO, and MB-rGO from aqueous suspensions. The room-temperature dried slides were further incubated at 50°C for 30 minutes to facilitate satisfactory surface adhesion of the graphene flakes, which otherwise showed tendency to lift off the substrate surface in aqueous environment. The physisorption of the rGO materials to the silica surface were the only stabilisation force: no chemical tethering was performed.

Seeded Array Patterning

The seed gold nanoparticles were prepared by a rapid sodium borohydride reduction of auric chloride in the presence of a

citrate surface ligand²⁸: 0.6 mL of ice-cold 0.1M NaBH_4 solution was quickly added while stirring to the 20 mL solution containing 2.5×10^{-4} M HAuCl_4 and 2.5×10^{-4} M sodium citrate. The resulting gold nanoparticles are spherical in shape with a diameter 4.3 ± 0.6 nm (TEM, size distribution histogram and UV-VIS spectrum is shown in supplemental material Fig. S1). The resulting gold colloid was left to mature for 2-3 hours before the printing step. The final concentration of the seed colloid is estimated as 55 ± 5 nM from the mass balance. Three concentrations of the seed nanoparticle colloid were inkjet printed in 12×8 rectangular array configuration on bare and GO/rGO coated glass substrates; a part of the developed array is shown in the Fig. 3 insert. The printed arrays were incubated for 48 hours allowing the seed particles to settle on the substrate surface. The concentration of the printed seed particles determines the subsequent surface number density of the grown particles.

Growth of Gold Nanoparticles on GO/rGO substrates

The growth of the printed gold seed nanoparticles forming the photonic surface was performed directly in the flow cell of the imaging instrument at $23 \pm 0.5^\circ\text{C}$. The growth solution was flowed over the surface at 0.1 mL/min, equivalent to a 2 mm/min linear flow rate. The flow conditions in the cell correspond to a laminar flow regime. The standard composition of the growth solution, $\times 1$ developer, is based on the gold rod nanoparticle synthesis protocol²⁸ previously optimised for our light scattering multiplexed biosensor array platform^{29,30}: 0.05 M CTAB, 2.5×10^{-4} M HAuCl_4 , 2×10^{-6} M AgNO_3 , and 4.5×10^{-4} M ascorbic acid. Bulk solution phase synthesis under these conditions leads to the formation of gold nanorods. In contrast, growth of the seed particles on the silica-water interface of the substrate surface results in nearly-spherical truncated polyhedral particles. Omission of the silver nitrate from the growth solution results in the formation of a small population of rods and flat polygonal particles³⁰. Several variations of the developer were used to study the effect of the HAuCl_4 concentration on the growth process. The concentration of the CTAB surfactant was kept constant at 0.05M.

The imaging platform is described in detail elsewhere²⁹. Briefly, the arrays are illuminated in near field following a total internal reflection event. Scattered light from a 635 nm LED is collected normal to the substrate surface by a video camera. Prior to surface synthesis the scattered light intensity from the seed nanoparticles is below the detection limit of the video camera. As the particles increase in diameter and scattering cross section, the scattered light intensity increases which allows the growth kinetics to be monitored in real time. The time-dependent responses from the 16 array spots printed with the same seed concentrations are averaged together, producing corresponding kinetic growth curves of the gold seed nanoparticles.

Biosensor Immunoassay

Several sensor arrays were used in immunoassay experiments to examine the effect of the graphene-coated substrate on the

assay performance. The detailed biosensor manufacturing procedure is described elsewhere²⁹. Briefly, the 12×8 rectangular sensor arrays were prepared by inkjet printing of the seed particles and developing them for 30 min in the growth solution as above. The gold nanoparticle surface was activated for protein binding using DTSP and the arrays were returned to the inkjet printer. Each array spot can be functionalized with different proteins under the registration control of the printer, forming the sensor that can potentially detect up to 96 analytes simultaneously. In the current study five proteins, aTRA, aCRP, protein A/G, TRA, and BSA, were used with repeats for bio-functionalization of the array spots. In immunoassay the arrays were initially stabilized in a flow of PBS buffer, then 200 nM anti-transferrin and 100 nM transferrin solutions were injected sequentially for ca. 10 minutes each with buffer wash steps in between the injections. Binding of the biomolecules on the sensor surface changes the local medium refractive index, which affects scattering properties of the gold nanoparticles, subsequently observed as change of the scattering brightness of the sensor array spots. The observed transient responses were averaged over the similarly bio-functionalized array spots.

Results and Discussion

The sensitivity and performance of an optical biosensor based on the plasmonic properties of the gold nanoparticles depends critically on the shape and size of these particles which can be optimised for a specific application. Chemical growth of the nanoparticles directly on the sensor substrate surface allows straightforward control of their location in an array format, their size and also their number densities. Whilst the number of the particles is determined by the seed particles concentration in the printed solution, their final size is a function of many parameters including temperature, chemical composition of the developer, chemical properties of the interface surface. Graphene is known to influence redox reactions³¹ and therefore it is expected that the growth of the gold particles by chemical reduction of the auric chloride would be modified by the presence of the graphene coated surfaces.

The experimental kinetic growth curves are recorded as change in the light scattering intensity, that can be converted into increasing mass of gold in the growing nanoparticles by making some assumptions about the evolution of optical properties with particle size. The grown particles are approximately spherical in shape and the scattering and absorption properties of spherical particles can be calculated using Mie theory, given a reasonable choice of the dielectric properties of the metal particle³². As a first approximation, the bulk gold permittivity can be used but when the size of the nanoparticles is smaller than the electron mean free path in bulk gold (~50 nm³³), the electron scattering from the particle boundary becomes significant and affects the dielectric function³⁴. The contribution of the bound electrons to the dielectric function is usually considered size-independent for particles larger than 2 nm, and only the free electrons contribution is taken as particle size dependent³². The complex dielectric function for

the free-electrons contribution is described by the following equation^{32, 33, 35}:

$$\epsilon_{free\ electrons}(\omega) = 1 - \frac{\omega_p^2}{\omega^2 + i\omega(\gamma_{bulk} + C\frac{\omega_F}{R})}$$

Equation 1

where ω_p is the bulk plasma frequency 13×10^{15} Hz, ω_F is the electron velocity at the Fermi surface 14.1×10^{14} nm s⁻¹, γ_{bulk} is the dumping constant for free electrons = 1.1×10^{14} Hz, R is the radius of the particle, and C is a constant associated with details of scattering processes was taken as 0.8³². The complex dielectric function depends on the particle size, with an approximate twofold increase in the imaginary part for 10 nm particles compared with the bulk metal value, whereas the real part changed by <1%, Fig. 1A. The imaginary part of the refractive index principally defines optical scattering properties of nanoparticles, so the temporal variation of the light scattering intensity will be a sensitive measure of the particle growth process on the substrates.

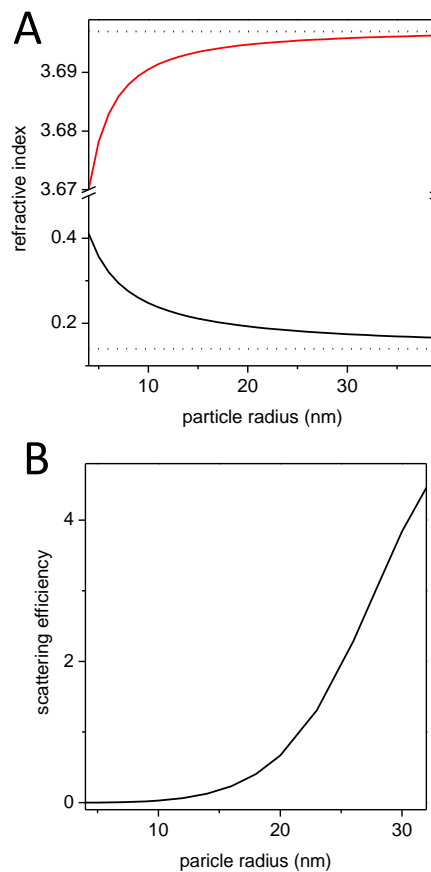


Fig. 1. Size dependence of optical properties of gold nanoparticles: (A) real (top) and imaginary (bottom) parts of the refractive index. The dotted lines refer to the respective bulk gold values; (B) scattering efficiency of nanoparticles in medium with RI of 1.3335 at 660 nm, corresponding to the kinetic particle growth experimental conditions: aqueous solutions and probe light wavelength.

After the particle size correction has been applied to the optical properties of the bulk gold³⁶, the corrected dielectric function

was converted to a size-dependent refractive index, Fig. 1A, and used in Mie theory calculations³⁷ to give the wavelength and particle-size dependent scattering efficiency, Fig. 1B. The latter was used to determine nanoparticle size from the experimentally observed light scattering data. The variation of the gold dielectric function with temperature is small and was neglected³³.

Assuming non-interacting particles, the overall observed scattering brightness is proportional to the number density of the particles on the sensor surface. Although a known concentration of the seed particles was printed per array spot, the total number present in the array spot depends on the surface ability to attract and immobilise particles from the printed colloid with a reasonable affinity.

The substrate arrays were imaged by scanning electron microscopy (SEM) at low resolution and large field-of-view settings after each of the growth experiments to determine the particle number density by counting the particles in several images, and the overall gold surface coverage as a bright fraction of the image area. Higher magnification images were used to measure the particle size distribution, Fig. 2.

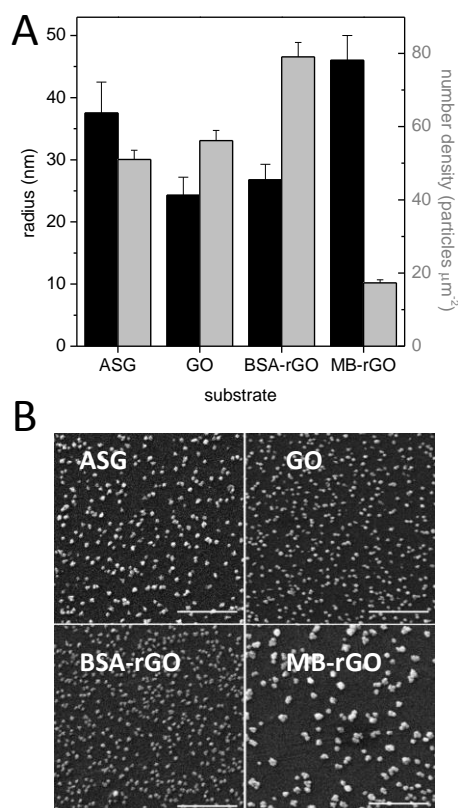


Fig. 2. (A) Surface number densities, grey, of the nanoparticles printed with stock 55nM seed colloid, and their sizes, black, observed in SEM image data after 40 minutes growth in the standard developer. (B) SEM images of the grown nanoparticles on different substrates, scale bar is 1 μm .

The overall gold surface coverage can also be calculated using the counted number density from low-resolution images and the

particle dimensions from high-resolution images. The gold surface coverages estimated by these two approaches are in good agreement (the correlation is shown in supplemental material Fig. S2).

The observed particle number densities on different substrates are shown in Fig. 2A. The BSA-rGO substrate supports the largest density of nanoparticles, up to 80 particles per μm^2 , reflecting the enhanced affinity of the seed particles for the protein surface²⁶. The lowest particle number density, about 18 particles per μm^2 , was observed on the MB-rGO substrate, potentially because it carries a strong negative charge from the methyl blue dye and therefore repels similarly charged colloidal gold particles. The array spots on the MB-rGO coated substrate also show small regions of very high particle density (supplemental Fig. S3), which are interpreted as gaps in the graphene layer where the bare, positively-charged aminated glass surface is exposed and captures the particles efficiently.

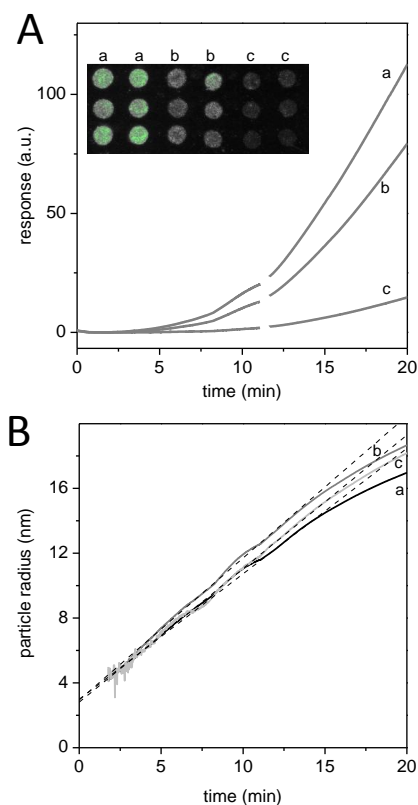


Fig. 3. Seed mediated growth of gold nanoparticles on the BSA-rGO substrate surface: (A) experimental kinetic traces corresponding to the three colloids which are printed with varying seed solution concentrations, a – 55 nM, b – 18 nM, and c – 6 nM, the insert shows part of the developed sensor image with printed spots, the sensor response is the brightness of the imaged array spots; (B) particle radii derived from the kinetic traces in A using the scattering efficiency shown in Fig. 1 and the final particle sizes and number densities measured from SEM images, dash lines are simulations.

Gold nanoparticle affinities for attachment of the nanoparticles to the GO/rGO surfaces were also checked in the absence of the substrate surface effects. In a separate experiment the graphene

material suspensions in water were incubated with gold colloid (15 nm diameter citrate reduced gold particles); only the BSA/FG-rGO samples effectively captured the gold particles, whereas GO and MB-rGO were hardly successful, in agreement with the behaviour observed on the sensor substrates (supplemental Fig. S4).

The solution concentration of the printed seed nanoparticles is the controlling factor in determining the final number of particles on the surface. Although the used concentrations were sequential three-fold dilutions of the stock 55 nM seed colloid (55, 18, and 6 nM), the observed surface number densities were not accurately proportional to the printed seed concentrations (supplemental Fig. S5). On the ASG, GO, and BSA-GO the lowest used concentration of seed colloid, 6 nM, deposited significantly less, ca. 50%, particles on the surface than expected comparing with the middle seed concentration, 18 nM. Similar effect was observed for the 55 nM and 18 nM printed seed concentrations on the MB-rGO sample. The effect limits the utility of the seed colloid concentration as a control for the desired surface density of the nanoparticles.

A simple description of the particle growth kinetics can be based on an assumption of either reactant diffusion or surface reaction limited mechanism. There is a large excess of the reagents in the bulk of the developer solution flow and their concentrations are treated as constant. The diffusion-limited growth mechanism would suggest a growth rate with a $time^{1/3}$ dependence. However, a surface reaction controlled growth would lead to a linear particle size increase with time.

All recorded kinetic traces display an initial fast scattering increase phase with further growth that shows approximately linear growth after 15 minutes, Fig. 3A. The observed growth behaviour is more consistent with the surface reaction limiting mechanism. A similar mechanism with a linear growth law was postulated in a study of gold nanoparticle growth in solution³⁴. There is an indication that growth rates slow down after 16-17 minutes, which may be associated with an onset of the reagent transport limiting kinetics. Fitting the initial 15 min period of the kinetic trace to a line function, Fig. 3B, results in a slope parameter describing the particle growth rate and an offset corresponding to the initial radius of the seed particles. The offset falls within the range 2.6-3.1 nm, in reasonable agreement with the known size distribution of the used seed particles, 4.3 ± 0.6 nm diameter. The linear growth rate has been derived for each surface and is presented in Fig. 4B.

The particle growth rates obtained for developer compositions with varying auric chloride concentration, Fig. 4A, show that the rate is approximately proportional to the concentration of gold ions in the developer within the range 0.1-0.5 mM, hence it can also be used as a growth rate control if required.

The ability to grow different shapes of nanoparticles on graphene substrates is significant advantage for metal-graphene nanocomposites in new applications^{14, 22}. The control of particle shape is, however, not straightforward and it is known that the bulk solution methods show different results in size and shape distributions compared with nanoparticles grown at the solid-liquid interface³⁰. The gold nanorods growth method with

CTAB surfactant²⁸, on which the current development is based, was also reported to produce rounder thorny/star-shaped gold nanoparticles³⁸ in slightly modified conditions (NaOH presence) which disturb CTAB binding. Application of the current development procedure results in nearly spherical particles, with some indication of sharper geometrical features forming at the later stages of growth (supplemental Fig. S6). If other shapes are desired then different development chemistry shall be used, for example decylpyrene surfactant was reported to be more effective in nanorod formation than CTAB when particles are grown on graphene surface²⁵.

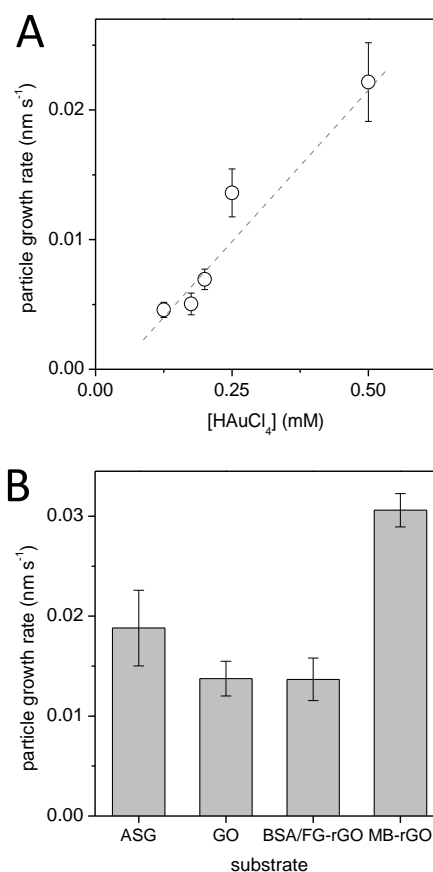


Fig. 4. Dependence of particle radius growth rate on (A) the concentration of auric chloride in the developer solution, and (B) the substrate surface coating.

The gold nanoparticle radius growth rates derived from the early-time kinetic traces are shown in Fig. 4B. The seed particles grow more slowly on the surface of graphene oxide and protein decorated reduced graphene oxide, compared to the reference aminated glass surface. By contrast, the growth rate is almost twofold increased on the surface of the methyl blue reduced graphene oxide. A tentative explanation might be related to the conductivity of the surface layer on which the seed particles are deposited: ASG and GO substrates are not conductive, and the protein decoration of the BSA-rGO layer may also prevent particle contact with the conductive rGO

sheet, whereas small aromatic methyl blue decoration of MB-rGO cannot shield the seed particle from interaction with conductive reduced graphene²⁷, which might serve as a source of electrons for redox growth process and/or reduce electrochemical potential for Au(I) reduction at the vicinity of the seed nanoparticle.

The total mass deposition rate may be derived from product of the density of gold and the change of nanoparticle volume per time when the particle surface number density and their size dependence on time are known. The derived growth rates and SEM data allow the average gold mass deposition rate on the substrate surface to be estimated as $< 6 \times 10^{-4} \text{ g cm}^{-2} \text{ h}^{-1}$ for the samples studied. This may be compared with the reported gold influx in the formation of dendritic gold nanostructures on graphene oxide surface of ca. $0.13 \text{ g cm}^{-2} \text{ h}^{-1}$ at 25 °C in a diffusion controlled growth process¹⁴. The two-hundred-fold slower gold influx estimated here is consistent with the reaction-limited rate at the beginning of the growth. The seed nanoparticle growth results in a ten-fold increase in the radius of the nanoparticle and consequent 100-fold increase in area and the transition to the diffusion-controlled growth mechanism. A consequence of the switch to diffusion controlled process is at the later stage of the growth, there is an observed inverse correlation between the final particle size and the number density of the nanoparticles on the surface.

The light-scattering properties of the sensor are a useful pointer to the sensitivity of a biosensor platform based on this detection event but an equal consideration is the bio-functionalization of the surface for label-free recognition of the target substrate. Thus the ultimate aim of the current study was to consider the potential of the graphene-composite materials in the production of biosensor surfaces in the array format multiplex biosensor. Despite differences in synthesis of the GO and MB-rGO substrates these surfaces showed no improvement over the biosensor arrays printed on the standard ASG substrate. In contrast, the BSA-rGO samples delivered important improvements in immunoassays, where antibodies are printed on the surface of the sensor to detect proteins in solution: a label-free protein screening array.

The biologically specific array sensors were fabricated with the following functionality: protein A/G, aTRA, TRA, aCRP, and BSA. The latter served as a non-specific reference in the course of the assay. At the end of the assay, the entire sensor surface was re-generated with an acid wash removing adsorbed proteins. The ASG sensor can be reused about 10 times with 2-5% performance loss per assay sequence. The BSA-rGO sensor was more susceptible to the degradation during the regeneration step, losing about half of the detection performance after a single regeneration step, probably due to denaturing of the protein coating on the graphene surface at the regeneration buffer pH.

The assay step sequence included injections of two analyte solutions, aTRA antibody (step 1, 0-10 min) and TRA (step 2, 28-38 min), with buffer washes between and a regeneration step at the end (step 3), Fig. 5. In assay step 1, the sensor channels with protein A/G and TRA respond to the injection of the

aTRA antibody, the former capturing immunoglobulin at Fc region, and the latter forming specific aTRA-TRA antibody-antigen complex. The aTRA antibodies bond to protein A/G via their nonspecific Fc region can still interact with antigen, therefore after the first step of the assay, 0-10 min, there are two TRA protein sensitive channels on the sensor: the aTRA-proteinA/G complex (b) and the originally printed aTRA (c), Fig. 5AB. Apart from the weaker, about twofold, overall response from BSA-rGO based sensor compared with the standard ASG the sensors performed similarly in the antibody capture assay step 1.

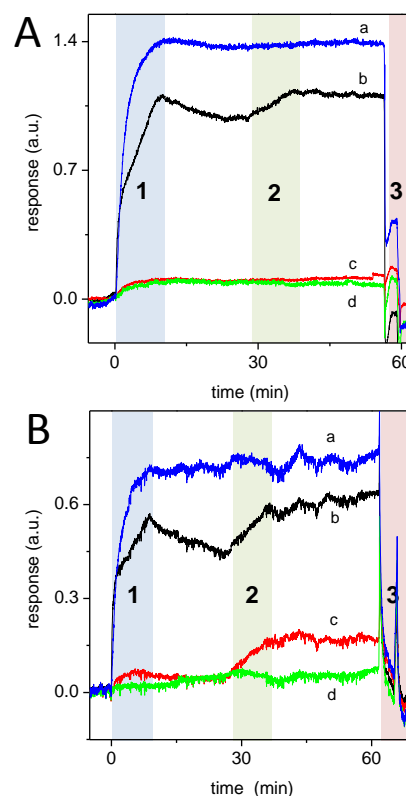


Fig. 5. TRA and aTRA kinetic immunoassays performed on the sensor arrays manufactured using ASG (A) and BSA-rGO (B) substrates and immobilized proteins TRA (a), protein A/G (b), aTRA (c), aCRP (d). aTRA antibody solution was injected at the start of the experiment (step 1 shaded area), it binds to the immobilized TRA (a) and is also captured by protein A/G (b). The TRA solution was injected at ca. 28 min (step 2 shaded area), resulting in evident sensor response in aTRA (c) and aTRA-protein A/G (b) channels on BSA-rGO substrate (B), but only the aTRA-protein A/G (b) channel showed any detectable response on the standard ASG substrate (A). The printed aTRA antibody (c) retained its activity only on BSA-rGO substrate. aCRP channel (d) is presented as a non-specific reference. Shaded area 3 marks the regeneration step. The sensor response corresponds to the relative change of brightness of the array spots.

In assay step 2, the injection of TRA analyte at ca 28 minutes is expected to be detected in both printed aTRA and captured aTRA-protein A/G channels, (c) and (b) in Fig. 5AB, respectively. The ASG sensor array responded only in aTRA-protein A/G channel (b) with ca. 30% activity determined from the ratio of the detected TRA to the captured antibody. In

contrast, no significant signal, <3%, was detected in printed aTRA channel (c), Fig. 5A, indicating that the printed aTRA antibody has lost its antigen recognition activity on ASG substrate. The sensor based on BSA-rGO substrate, however, showed about 60% activity of the aTRA-protein A/G channel and, more importantly, it also showed similar activity in the printed aTRA channel, Fig. 5B(c), implying that the BSA-rGO surface is approximately 20-fold more effective (60% against <3%) in maintaining the activity of the immobilized aTRA antibody printed onto the array at the sensor fabrication stage. The assays limit of detection towards TRA is estimated as 9 nM (sensor response rising above 2σ of the noise level after 10 min analyte injection), with a dynamic range 9–3000 nM.

Conclusions

Several substrates coated with thin layer of graphene materials were studied as candidates for spatially controlled gold nanoparticle growth with ultimate target of their usage as multiplex biosensors. Both the deposition of the seed nanoparticles and the kinetics of the seed mediated particle growth were influenced by the surface functionalization with graphene samples. The rates of the particle growth indicate that the process is reaction controlled at the employed experimental conditions on all tested surfaces. The choice of the surface coating and the development conditions (concentration of printed seed particles, chemical composition of the growth solution, development time) allow some control over the surface number density and size of the grown particles. Among the tested samples the BSA reduced graphene oxide coated substrate appears to be a promising candidate as a base for antigen capture array biosensors, although further optimisation of the overall sensor sensitivity and stability is desired. The presented results can also be useful in other surface sensitive applications, e.g. SERS or SPR.

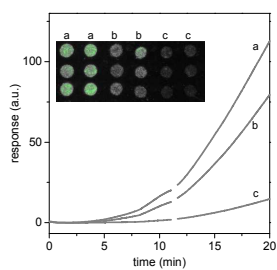
Notes and references

^a College of Life and Environmental Sciences, University of Exeter, Stocker Road, Exeter, EX4 4QD, United Kingdom

Electronic Supplementary Information (ESI) available. See DOI: 10.1039/b000000x/

- M. U. Ahmed, I. Saaem, P. C. Wu and A. S. Brown, *Crit. Rev. Biotechnol.*, 2013, 1-17.
- D. J. Brennan, D. P. O'Connor, E. Rexhepaj, F. Ponten and W. M. Gallagher, *Nat. Rev. Cancer*, 2010, **10**, 605-617.
- J. D. Hoheisel, M. S. S. Alhamdani and C. Schröder, *Prot. Clin. Appl.*, 2013, **7**, 8-15.
- H. Sun, Grace Y. J. Chen and Shao Q. Yao, *Chem. Biol.*, 2013, **20**, 685-699.
- W. Hong, H. Bai, Y. Xu, Z. Yao, Z. Gu and G. Shi, *J. Phys. Chem. C*, 2010, **114**, 1822-1826.
- S. Mao, G. Lu, K. Yu, Z. Bo and J. Chen, *Adv. Mater.*, 2010, **22**, 3521-3526.
- W. Song, D.-W. Li, Y.-T. Li, Y. Li and Y.-T. Long, *Biosensors Bioelectron.*, 2011, **26**, 3181-3186.
- C.-F. Huang, G.-H. Yao, R.-P. Liang and J.-D. Qiu, *Biosensors Bioelectron.*, 2013, **50**, 305-310.
- V. K. Gupta, M. L. Yola, M. S. Qureshi, A. O. Solak, N. Atar and Z. Üstündağ, *Sens. Actuators, B*, 2013, **188**, 1201-1211.
- H. Wu, J. Wang, X. Kang, C. Wang, D. Wang, J. Liu, I. A. Aksay and Y. Lin, *Talanta*, 2009, **80**, 403-406.
- F. Li, Z. Wang, C. Shan, J. Song, D. Han and L. Niu, *Biosensors Bioelectron.*, 2009, **24**, 1765-1770.
- D. Saini, R. Chauhan, P. R. Solanki and T. Basu, *ISRN Nanotechnology*, 2012, **2012**.
- Q. Xi, X. Chen, D. G. Evans and W. Yang, *Langmuir*, 2012, **28**, 9885-9892.
- K. Jasuja and V. Berry, *ACS Nano*, 2009, **3**, 2358-2366.
- Y. Zhang, S. Liu, L. Wang, X. Qin, J. Tian, W. Lu, G. Chang and X. Sun, *RSC Advances*, 2012, **2**, 538-545.
- S. Salgado, L. Pu and V. Maheshwari, *J. Phys. Chem. C*, 2012, **116**, 12124-12130.
- P. V. Kamat, *J. Phys. Chem. Lett.*, 2009, **1**, 520-527.
- F. Bei, X. Hou, S. L. Y. Chang, G. P. Simon and D. Li, *Chem. Eur. J.*, 2011, **17**, 5958-5964.
- S. Watcharotone, D. A. Dikin, S. Stankovich, R. Piner, I. Jung, G. H. B. Dommett, G. Evmenenko, S.-E. Wu, S.-F. Chen, C.-P. Liu, S. T. Nguyen and R. S. Ruoff, *Nano Lett.*, 2007, **7**, 1888-1892.
- F. Xiao, J. Song, H. Gao, X. Zan, R. Xu and H. Duan, *ACS Nano*, 2011, **6**, 100-110.
- B.-S. Kong, J. Geng and H.-T. Jung, *Chem. Commun.*, 2009, 2174-2176.
- Y. H. Lee, L. Polavarapu, N. Gao, P. Yuan and Q.-H. Xu, *Langmuir*, 2011, **28**, 321-326.
- M. Liu, H. Zhao, S. Chen, H. Yu and X. Quan, *ACS Nano*, 2012, **6**, 3142-3151.
- R. Muszynski, B. Seger and P. V. Kamat, *J. Phys. Chem. C*, 2008, **112**, 5263-5266.
- Y.-K. Kim, H.-K. Na and D.-H. Min, *Langmuir*, 2010, **26**, 13065-13070.
- J. Liu, S. Fu, B. Yuan, Y. Li and Z. Deng, *J. Am. Chem. Soc.*, 2010, **132**, 7279-7281.
- X. Cai, S. Tan, A. Xie, M. Lin, Y. Liu, X. Zhang, Z. Lin, T. Wu and W. Mai, *Mater. Res. Bull.*, 2011, **46**, 2353-2358.
- C. J. Murphy, T. K. Sau, A. M. Gole, C. J. Orendorff, J. Gao, L. Gou, S. E. Hunyadi and T. Li, *J. Phys. Chem. B*, 2005, **109**, 13857-13870.
- R. V. Olkhov, J. D. Fowke and A. M. Shaw, *Anal. Biochem.*, 2009, **385**, 234-241.
- R. V. Olkhov and A. M. Shaw, *Biosensors Bioelectron.*, 2008, **23**, 1298-1302.
- G. Shi, Z. Wang, J. Xia, J. Tang, F. Zhang, Y. Li, Y. Xia and L. Xia, *Int. J. Electrochem. Sci.*, 2013, **8**, 8764-8773.
- L. B. Scaffardi and J. O. Tocho, *Nanotechnology*, 2006, **17**, 1309.
- S. Link and M. A. El-Sayed, *J. Phys. Chem. B*, 1999, **103**, 4212-4217.
- R. D. Averitt, D. Sarkar and N. J. Halas, *Phys. Rev. Lett.*, 1997, **78**, 4217-4220.
- U. Kreibig and L. Genzel, *Surf. Sci.*, 1985, **156**, Part 2, 678-700.

36. P. B. Johnson and R. W. Christy, *Physical Review B*, 1972, **6**, 4370-4379.
37. I. Charamisinau, G. Happawana, G. Evans, A. Rosen, Richard A. Hsi and D. Bour, *Appl. Opt.*, 2005, **44**, 5055-5068.
38. C. L. Nehl, H. Liao and J. H. Hafner, *Nano Lett.*, 2006, **6**, 683-688.



Gold nanoparticles were seed-mediated grown on graphene coated substrates and resulting composites were employed in light-scattering imaging biosensor immunoassay application.